Strain-engineering stabilization of $BaTiO_3$-based polar metals

Chao Ma,[1,2] Kui-juan Jin,[1,2,3,*] Chen Ge,[1] and Guo-zhen Yang[1,2,3]

[1]*Beijing National Laboratory for Condensed Matter Physics, Institute of Physics, Chinese Academy of Sciences, Beijing 100190, China*

[2]*School of Physical Sciences, University of Chinese Academy of Sciences, Beijing 100190, China*

[3]*Collaborative Innovation Center of Quantum Matter, Beijing 100190, China*

(Received 27 November 2017; revised manuscript received 5 January 2018; published 1 March 2018)

Polar metals, which possess ferroelectriclike polar structure and conductivity simultaneously, have attracted wide interest since the first solid example, $LiOsO_3$ (below 140 K), was discovered. However, the lack of room-temperature polar metals hinders further research and applications. Thus abundant properties of polar metals are unexplored. Here, with first-principles calculations, we report that the polar metal phase can be stabilized in the strain-engineered $BaTiO_3$ with electron doping. The mechanism relates to the competition between the shifting of the t_{2g} energy levels and the narrowing of their bandwidth. Surprisingly, it is predicted that the ferroelectric-to-paraelectric transition temperature can be increased by electron doping when the strain is large enough, which holds potential for room-temperature polar metals. Our results indicate that strain engineering is a promising way to achieve $BaTiO_3$-based polar metals, and they should have practical significance for obtaining easily accessible, ecofriendly, and potential room-temperature polar metals.

DOI: 10.1103/PhysRevB.97.115103

I. INTRODUCTION

The concept of "ferroelectric metal" was put forward by Anderson and Blount [1] about half a century ago. $LiOsO_3$, as the first solid proof of a polar metal [2], which is a metal but undergoes a ferroelectriclike phase transition around 140 K, has inspired numerous studies recently [3–13]. Aside from the potentially unusual properties [14–18], the most interesting part about polar metals is that the free carriers and unscreened long-range ordered dipoles could coexist. Considering the origin of ferroelectricity, Puggioni and Rondinelli [19] proposed that the polar metals should satisfy the "weak coupling" between the free electrons at the Fermi level and the soft mode phonons which lead to the polar structure.

The intrinsic polar metals are extremely rare. We summarize that the alternative way is to design polar metals by considering the weak-coupling rule as manifested in Fig. 1, by inducing a polar structure in a metal, or by introducing itinerant carriers into a ferroelectric (FE) material. "Geometric design" was proposed to fulfill the former way; taking the $ANiO_3$-based polar metals as an example, the cooperative polar A cation displacements are geometrically stabilized, while the partially occupied band of Ni provides metallicity [13]. Here we focus on the latter way. Since the low to high symmetry transition induced by electron doping seems very general [20], the major problem is how to keep the polar distortion of the ferroelectric material while increasing the dope concentration. Recently, we have proposed that "lone-pair" [21,22] ferroelectric materials, such as $PbTiO_3$, are promising candidates for polar metals according to our first-principles investigations [23,24]. The polar distortion was found not only to be persisting, but was also being enhanced by the electron doping [23]. The weak-coupling mechanism makes sure that the free carriers that are doped leave the long-range Coulomb interaction unscreened in lone-pair ferroelectrics [24]. Very recently, we have reported a room-temperature realization of a polar metal by fabricating a series of Nb-doped $PbTiO_3$ thin films [25]. The temperature-dependent resistivity of the $PbTi_{0.88}Nb_{0.12}O_3$ film showed a metallic feature, while the scanning transmission electron microscopy images clearly manifested the polar distortion. However, the volatility of the lead and its environmental issues restrict the fabrication and application for doped $PbTiO_3$.

$BaTiO_3$, as another traditional ferroelectric perovskite, does not suffer from these problems. It has been found that the polarization and the ferroelectric-to-paraelectric transition temperature (T_C) for *undoped* $BaTiO_3$ [26] and $BiFeO_3$ [27] films are enlarged by compressive strain. However, Nb-doped $BaTiO_3$ thin films have been studied experimentally for about 10 years, but they are mostly reported on for the metal-insulator transitions [28,29]. Recently, both theoretical works [30,31] and experimental ones [32–34] have stressed that the electron doping in $BaTiO_3$ screens the long-range Coulomb interaction and suppresses the polar distortion, indicating doping $BaTiO_3$ may not be suitable for obtaining polar metals. On the other hand, very recently, Takahashi *et al.* [35] have found a few signs that the polar phase might coexist with the metallic La-doped $BaTiO_3$ thin films on $GdScO_3$ substrates using second-harmonic generation measurement, but more evidence, such as scanning transmission electron microscopy measurement or theoretical proving, is needed to confirm the existence of the polar metal phase.

In this paper, by using standard density functional theory (DFT) calculations (see the Supplemenatal Material [36], and also Refs. [35,37–40]), we studied the combined effects of the electrostatic doping and the compressive strain in $BaTiO_3$. The fully relaxed crystal unit cell of $BaTiO_3$ without strain or doping is shown in Fig. 2(a). The in-plane and out-of-plane lattice

*kjjin@iphy.ac.cn

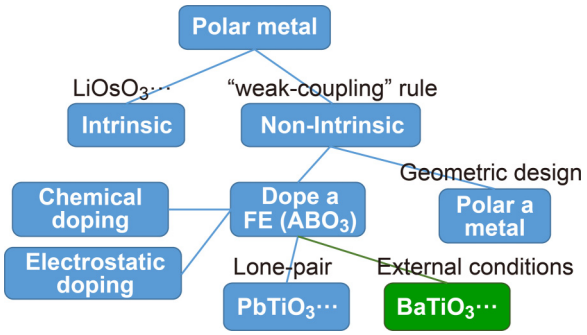

FIG. 1. The diagram for the routine to obtain polar metals.

constants are taken as 3.973 and 4.067 Å, respectively, which are in good agreement with the room-temperature experimental values (3.992 and 4.036 Å) [35], respectively, considering the thermal expansion. To simulate the biaxial strain imposed by the substrate, we fully relax the lattice subjected to a constraint on the in-plane lattice constant. $BaTiO_3$ has transitions to rhombohedral and orthorhombic phases at low temperature. It is important to consider all the possible structures from the material's design perspective. However, based on previous studies on the phase diagrams of $BaTiO_3$ under epitaxial constraints [41,42], the only phase transition that should be considered is that from the ferroelectric $P4mm$ phase to the paraelectric $P4/mmm$ phase if the compressive strain is larger than -1% (corresponds to the in-plane lattice constant $a < 3.94$ Å from our calculation). Therefore, only the tetragonal $P4mm$ phase and compressive strains are considered here. The doping electrons are introduced to the system with a uniform, positive background to achieve charge neutrality. We will show that the polar metal phase can be stabilized under compressive strain, and then how the strain affects the polar metal phase. The mechanism of why and how the polar metal phase can be stabilized by the strain will be demonstrated in the last part of the Results section. Our findings will add the routine of $BaTiO_3$-based (and other non-lone-pair ferroelectric-based) polar metals in Fig. 1, but with external conditions such as strain engineering.

II. RESULTS AND DISCUSSIONS

A. Combined effects of strain and doping

As the ferroelectric polarization is an ill-defined quantity in metallic materials, here we define a new physical parameter P' to characterize the polar distortion in electrostatically doped $BaTiO_3$,

$$P' = \frac{B_l - B_s}{B_l + B_s} = \frac{B_l - B_s}{c},$$

where B_l and B_s represent the long and short Ti-O1 bond lengths, respectively, shown in Fig. 2(a); c denotes the out-of-plane lattice constant. P' mainly reflects the extent of polar distortion. Larger P' represents larger polar distortion. If P' is 0, the structure stays in highly symmetric phase with no polar distortion. In addition, the quantity $(B_l - B_s)$ is plotted in Fig. S1 in the Supplemental Material [36] for obtaining the Ti off-centering more intuitively. We also define an energy difference dE, with $dE = E_{P4/mmm} - E_{P4mm}$, where $E_{P4/mmm}$ and E_{P4mm} represent the total energy corresponding to the highly symmetric tetragonal phase ($P4/mmm$) and the polar phase ($P4mm$) under compressive strain, respectively. Larger dE means a more difficult transition from $P4mm$ to $P4/mmm$, which indicates a more stable polar structure of the $P4mm$ phase. Larger dE also infers a larger T_C, which can be understood as a completely thermal activation mechanism. Therefore, the amplitude of dE serves to characterize the stability of the $P4mm$ phase and the qualitative trend of T_C. In order to clearly demonstrate that the polar metal phase can be stabilized by the strain, we also define a critical dope concentration n_C, beyond which $P' = 0$.

To obtain the combined effects of strain engineering and electrostatic doping on the polar distortion and the stability of $BaTiO_3$-based polar metals, we computed P' and dE shown in Figs. 2(b) and 2(c), respectively, as functions of the electrostatic dope concentration n_e and the in-plane lattice

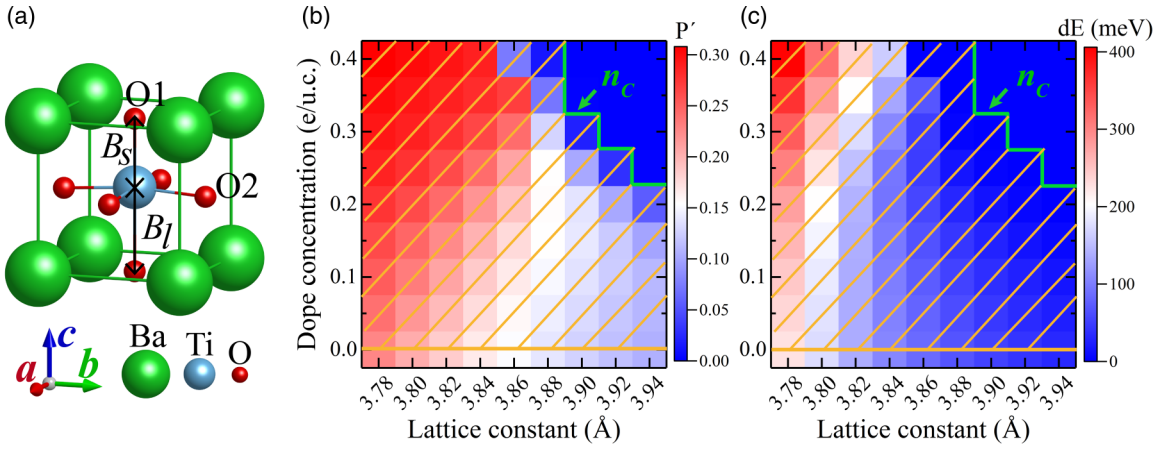

FIG. 2. The calculated $BaTiO_3$ crystal unit cell (a), where B_s and B_l represent the short and long Ti-O1 bond lengths, respectively. The heat map diagrams of P' (b) and dE (c), respectively, as functions of the dope concentration n_e and the in-plane lattice constant a, where $dE = E_{P4/mmm} - E_{P4mm}$. Green line in (b) represents the critical concentration n_C, beyond which $P' = 0$. Orange shadow in (b),(c) represents the region for obtaining the polar metal phase with nonzero n_e and P'.

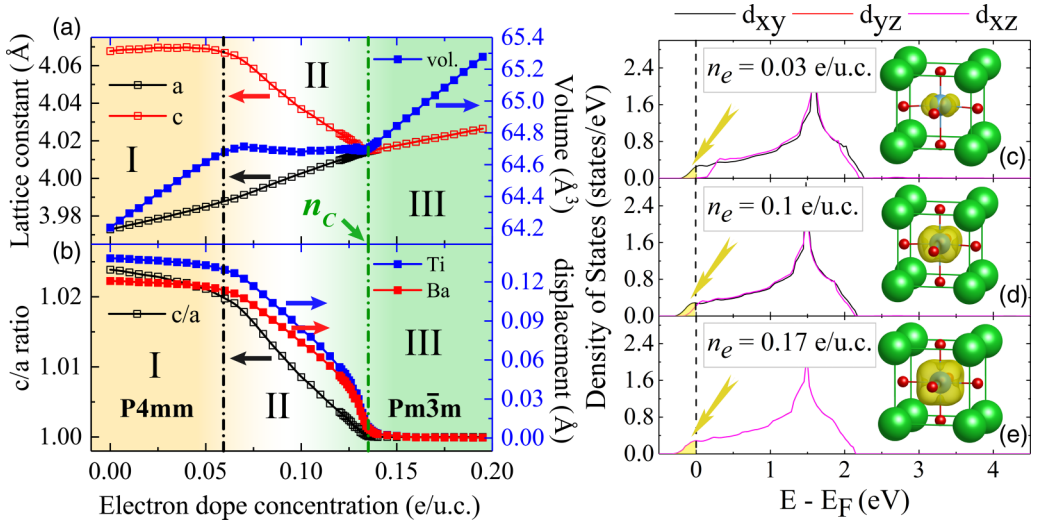

FIG. 3. (a) a, c, and unit cell volume versus n_e. (b) The ratio c/a and cation-oxygen relative displacements versus n_e. In (a),(b), the squares are calculated results. The dashed lines represent the boundaries of two adjacent regions, in which the green one also represents the critical concentration n_C. Orbital resolved DOS of three t_{2g} orbitals with n_e equals 0.03 e/u.c. (c), 0.1 e/u.c. (d), and 0.17 e/u.c. (e), corresponding to the regions I–III in (a),(b), respectively. In (c)–(e), the zero point of energy is placed at the Fermi level (E_F). The yellow areas with yellow arrows represent the doping electrons. The isosurface demonstration of charge density distributions of the doping electrons is drawn with the same scale in the inserted pictures. Note that the DOS of d_{yz} and d_{xz} orbitals always overlaps because these orbitals are degenerate due to the crystal symmetry.

constant a. Note that in our calculation, $a = 3.78$ Å is close to a -5% compressive strain which is difficult to achieve by epitaxial growth. We hope these results could shed some light on obtaining polar metals in some other ways such as high-pressure experiments or using other materials. The critical dope concentration n_C is denoted as the green lines in Figs. 2(b) and 2(c). It is found very promising that a large region shown as the orange shadow in Figs. 2(b) and 2(c) can be engineered to obtain a polar metal. In addition, the phase diagrams in Refs. [41,42] indicate that T_C in undoped $BaTiO_3$ increases with larger compressive strains, which agrees with the trend of $dE(n_e = 0)$ in Fig. 2(c). From Fig. 2(b), we can see that when a is within 3.86–3.94 Å, electron doping enhances the polar distortion (with increased P') at lower doping level, then reduces the polar distortion (with decreased P') at higher doping level. When a is smaller than 3.86 Å, electron doping within 0.4 e/u.c. (electrons per unit cell) will always enhance the polar distortion (with increased P'). Furthermore, compressive strain (with decreased a) enhances the polar distortion (with increased P') for any dope concentration. It is also worth noticing that n_C is increased significantly by compressive strain, which even exceeds 0.4 e/u.c. with a less than 3.9 Å. From Fig. 2(c), we can see that the stability parameter dE of the $P4mm$ phase (polar metal phase with a nonzero electrostatic doping) shows similar trends, as well as T_C. The stability is always weakened by doping with lattice constant a larger than 3.86 Å (with decreased dE). This should account for the monotonously decreased T_C of $BaTiO_3$ with increasing La doping on the $GdScO_3$ substrate (3.970 Å) [35]. Surprisingly, when a is smaller than 3.86 Å, the stability can be improved by doping (with increased dE), as shown in Fig. 2(c). Therefore, we predict that T_C can be increased by low doping with a large compressive strain, indicating a potential room-temperature polar metal.

B. Weak-coupling region

To understand why the compressive strain can stabilize the polar metal phase in $BaTiO_3$, we start with reviewing the electrostatic doping effects without strain. The evolution of the $BaTiO_3$ unit cell structure as a function of electron doping is illustrated in Figs. 3(a) and 3(b). Trends of the c/a ratio and cation-oxygen relative displacements are in agreement with previous reports [30,31]. Here, the critical concentration n_C is about 0.134 e/u.c. (2.0×10^{21} cm^{-3}) from our calculations, being slightly larger than the reported 0.11 e/u.c. (1.9×10^{21} cm^{-3}) [29], caused by different computational methods. N_C also indicates a transition concentration from region II to III, denoted by the green line in Figs. 3(a) and 3(b). Apart from the similarities, a distinct terrace of the volume curve in Fig. 3(a) is identified. The unit cell volume does not keep growing with increasing the dope concentration. Instead, it is nearly unchanged within the doping range around 0.06–0.134 e/u.c. ($0.93-2.0 \times 10^{21}$ cm^{-3}) denoted as region II in Fig. 3(a). Meanwhile, the polar distortion decreases dramatically in this region, which is, however, nearly unaffected with a lower dope concentration, as shown by the Ti-O and Ba-O relative displacements in region I of Fig. 3(b).

To demonstrate the mechanism of the structure deformation behavior with doping, the orbital resolved density of states (DOS) for Ti atoms with various doping densities is drawn in Figs. 3(c)–3(e). As three t_{2g} orbitals (d_{xy}, d_{yz}, and d_{xz}) of the center cation (Ti) in the oxygen octahedron configuration have the lowest energy among the five $3d$ orbitals, and the electronic states of the Ti $3d_{xy}$ orbital locate at the conduction band minimum (CBM) due to the polar distortion along the c axis, the electrons doped only distribute in the d_{xy} orbital when the doping level is very low, as shown in Fig. 3(c). We find the screening from these electrons is so anisotropic that the c-oriented polarization is hardly affected, which is similar to

that in the electron-doped lone pair $SnTiO_3$ [24]. These results indicate that there is very little coupling between the conduction electrons at the Fermi level and the soft mode phonons for generating the polar structure in this case. This weak-coupling region at low doping density is marked by region I in Figs. 3(a) and 3(b), explaining why the polar distortion seems unaffected by doping. With increasing dope concentration [marked by region II in Figs. 3(a) and 3(b)], the electrons start to fill in the d_{yz}/d_{xz} states, and the charge density distribution of doping electrons tends to be a little isotropic, as shown in Fig. 3(d). The screening of c-oriented polarization reduces the polar displacements and the out-of-plane lattice constant dramatically, as shown in Figs. 3(a) and 3(b). Therefore, although the in-plane lattice constant keeps increasing with doping, the volume remains unchanged and forms a terrace in region II [Fig. 3(a)]. When the dope concentration further rises and reaches n_C, the screening becomes completely isotropic as manifested in Fig. 3(e), and the $P4mm$ phase transforms into the $Pm\bar{3}m$ cubic phase as shown in region III in Figs. 3(a) and 3(b).

To further confirm the weak-coupling feature, we conduct the following analysis, based on the well accepted understanding that the covalence Ti-O bonding interaction is the driving force of ferroelectric distortion, resulting in the soft modes in the highly symmetric cubic structure [43,44]. The DOS of the total unit cell and Ti $3d$ orbitals with various doping densities is plotted in Fig. S2 in the Supplemental Material [36], from which we can see that the Ti-O hybridization mainly locates within -6.5 to -3.5 eV below the Fermi energy. The corresponding real-space charge density distribution with various doping densities is illustrated in Fig. S3 in the Supplemental Material [36]. The distinct covalence bonding feature between the center Ti atom and surrounding O atoms with very low doping [0.03 e/u.c. as shown in Fig. S3(b)] is not weakened as compared to the undoped case [Fig. S3(a)], nor is the driving force of the polar distortion, showing a weak-coupling feature. However, the covalence bonding feature disappears in Figs. S3(c) and S3(d), in agreement with the feature in Figs. 3(a) and 3(b).

C. Strain-engineering stabilization of polar metal phase

To reveal why strain can stabilize $BaTiO_3$-based polar metals, we present the subtle relationship between the shift of the t_{2g} energy levels and the narrowing of their bandwidth in Fig. 4.

As aforementioned, the energy of the d_{xy} orbital is lower than those of the d_{yz}/d_{xz} orbitals. With compressive strain, the decrease of in-plane lattice constant a enlarges the out-of-plane lattice constant c. The change of the oxygen octahedron crystal field shifts the energy of the Ti $3d$ orbitals correspondingly. The energy level of the d_{xy} orbital is raised, while the d_{yz}/d_{xz} orbitals gain energy and are decreased. Thus the energy interval between the d_{xy} and d_{yz}/d_{xz} orbitals becomes smaller with compressive strain, which should reduce the d_{xy} proportion at the CBM, as schematically demonstrated in Fig. 4(a). On the other hand, the bandwidth of the d_{yz}/d_{xz} orbitals is markedly narrowed due to the diminished overlap between the wave functions along the z direction with enlarged lattice constant c. From Figs. 4(b)–4(d), we can also clearly see the narrowing

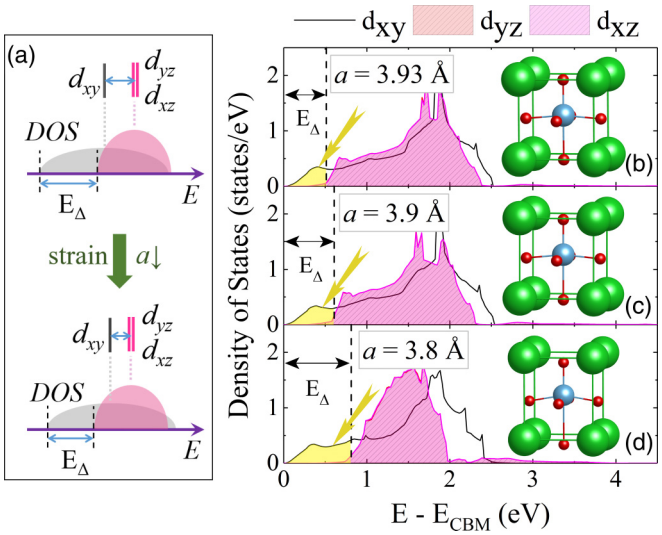

FIG. 4. (a) Diagram of the t_{2g} levels shifting and the consequent DOS shifting without narrowing of bandwidth with strain. The calculated orbital resolved DOS of three t_{2g} orbitals with a equals 3.93 Å (b), 3.9 Å (c), and 3.8 Å (d), respectively, without doping. E_Δ denotes the energy difference of the band bottoms for d_{yz}/d_{xz} with respect to that for d_{xy}. In (b)–(d), the zero point of energy is placed at the CBM. The yellow areas with yellow arrows schematically represent the doping range corresponding to the weak-coupling region. The inserted pictures show the corresponding unit cell structures. The d_{yz} and d_{xz} orbitals are degenerate, so their DOS always overlaps.

of the DOS for d_{yz}/d_{xz} orbitals with decreased lattice constant a. The amplitude of bandwidth narrowing is much larger than the shift of energy levels with application of a compressive strain, resulting in a larger energy difference E_Δ of band bottoms for the d_{yz}/d_{xz} with respect to that for the d_{xy} (CBM). Therefore, the CBM has more d_{xy} feature when applying a larger compressive strain, which equivalently extends the width of the weak-coupling region [region I in Figs. 3(a) and 3(b)], making the polar distortion unaffected in a larger doping range. Moreover, the doping electrons mainly distribute on Ti, which increases the Coulomb electrostatic repulsion between the Ti cation and O anions, and enlarges the average bond length of the Ti-O bonds. The constraint of the in-plane lattice constant further enlarges the lattice constant c, making the above mechanism more robust.

To further confirm the above mechanism, two sets of DOS demonstrations that include electron doping and epitaxial strain are plotted in Fig. 5. With a being fixed to be 3.88 Å, as n_e increases from 0.25 to 0.35 e/u.c., the polar distortion decreases as shown in Fig. 2(b). From the calculated DOS illustrated in Figs. 5(a)–5(c), we can see that more electrons are doped into d_{yz}/d_{xz} states, indicating the doping level shifts from region I to region II. Thus 0.3 e/u.c. approximately represents the boundary between regions I and II. Then, with n_e being fixed to be 0.3 e/u.c., as a decreases from 3.90 to 3.86 Å, the polar distortion increases as shown in Fig. 2(b). From Figs. 5(d)–5(f), we can see that the bandwidth of the d_{yz}/d_{xz} orbitals is dramatically narrowed, eventually leaving almost all the doping electrons distributed in the d_{xy} states only, which indicates the doping level shifts from region II to region I.

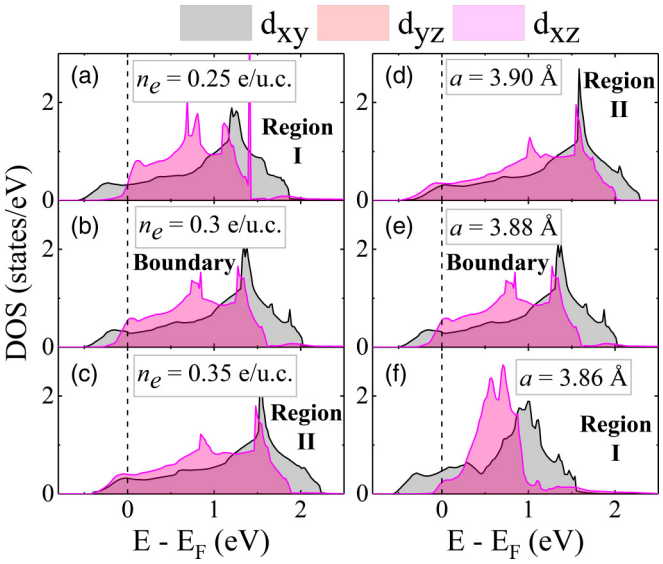

FIG. 5. The calculated orbital resolved DOS of three t_{2g} levels with in-plane lattice constant $a = 3.88$ Å but various doping (a)–(c) and with $n_e = 0.3e$/u.c. but various a (d)–(f). The zero point of energy is placed at the Fermi level (E_F). The d_{yz} and d_{xz} orbitals are degenerate, so their DOS always overlaps.

Therefore, the above results agree well with the mechanism we proposed.

To summarize, with compressive strain, the electronic structure favors stabilization of the polar metal phase by enlarging the doping range of the weak-coupling region, due to the much more remarkable bandwidth narrowing than the energy levels' shifting.

III. SUMMARY

In conclusion, by using DFT calculations, we conduct theoretical investigations on the combined effects of in-plane biaxial compressive strain and electrostatic doping on the polar distortion and the stability of $BaTiO_3$-based polar metals. Critical concentration with various strains has been proposed to achieve polar metal phase. It is found to be very promising that with a large range of dope concentrations and kinds of substrates (with a smaller lattice constant than $BaTiO_3$), $BaTiO_3$ can be engineered into a polar metal. Moreover, the stability of the polar metal phase is found to be significantly improved by strain engineering. Surprisingly, it is predicted that the ferroelectric-to-paraelectric transition temperature (T_C) should be improved by electron doping with a large enough strain, indicating $BaTiO_3$-based room-temperature polar metals are potentially achievable. To understand why the compressive strain can stabilize the polar metal phase, the crystal structure evolution behavior versus doping without strain in $BaTiO_3$ is reviewed, and a weak-coupling region is identified with low doping densities; it is found that the compressive strain can enlarge the doping range of the weak-coupling region. Furthermore, the strain-engineering stabilization of the $BaTiO_3$-based polar metal phase is explained from the electronic structure perspective, and the mechanism behind it is revealed as the dominated narrowing for the t_{2g} bandwidth.

Our results indicate that strain engineering is a promising way to achieve $BaTiO_3$-based polar metals. We believe these findings will contribute to the fabrication and application of easily accessible, ecofriendly, and potential room-temperature polar metals, and further facilitate the exploration of more abundant and fascinating properties of polar-metal-based devices.

ACKNOWLEDGMENTS

This work was supported by the National Key Basic Research Program of China (Grant No. 2014CB921001), the National Key Research and Development Program of China (Grant No. 2017YFA0303604) the Key Research Program of Frontier Sciences of the Chinese Academy of Sciences (Grant No. QYZDJ-SSW-SLH020), the Strategic Priority Research Program (B) of the Chinese Academy of Sciences (Grant No. XDB07030200), and the National Natural Science Foundation of China (Grants No. 11721404, No. 11674385, and No. 11404380).

[1] P. W. Anderson and E. I. Blount, Phys. Rev. Lett. **14**, 217 (1965).
[2] Y. Shi, Y. Guo, X. Wang, A. J. Princep, D. Khalyavin, P. Manuel, Y. Michiue, A. Sato, K. Tsuda, S. Yu, M. Arai, Y. Shirako, M. Akaogi, N. Wang, K. Yamaura, and A. T. Boothroyd, Nat. Mater. **12**, 1024 (2013).
[3] G. Giovannetti and M. Capone, Phys. Rev. B **90**, 195113 (2014).
[4] H. Sim and B. G. Kim, Phys. Rev. B **89**, 201107(R) (2014).
[5] H. J. Xiang, Phys. Rev. B **90**, 094108 (2014).
[6] C. He, Z. Ma, B.-Z. Sun, Q. Li, and K. Wu, Comput. Mater. Sci. **105**, 11 (2015).
[7] H. M. Liu, Y. P. Du, Y. L. Xie, J. M. Liu, C.-G. Duan, and X. Wan, Phys. Rev. B **91**, 064104 (2015).
[8] D. Puggioni, G. Giovannetti, M. Capone, and J. M. Rondinelli, Phys. Rev. Lett. **115**, 087202 (2015).
[9] N. A. Benedek and T. Birol, J. Mater. Chem. C **4**, 4000 (2016).
[10] F. Jin, A. Zhang, J. Ji, K. Liu, L. Wang, Y. Shi, Y. Tian, X. Ma, and Q. Zhang, Phys. Rev. B **93**, 064303 (2016).
[11] I. Lo Vecchio, G. Giovannetti, M. Autore, P. Di Pietro, A. Perucchi, J. He, K. Yamaura, M. Capone, and S. Lupi, Phys. Rev. B **93**, 161113(R) (2016).
[12] A. Filippetti, V. Fiorentini, F. Ricci, P. Delugas, and J. Iniguez, Nat. Commun. **7**, 11211 (2016).
[13] T. H. Kim, D. Puggioni, Y. Yuan, L. Xie, H. Zhou, N. Campbell, P. J. Ryan, Y. Choi, J. W. Kim, J. R. Patzner, S. Ryu, J. P. Podkaminer, J. Irwin, Y. Ma, C. J. Fennie, M. S. Rzchowski, X. Q. Pan, V. Gopalan, J. M. Rondinelli, and C. B. Eom, Nature **533**, 68 (2016).
[14] V. M. Edelstein, Phys. Rev. B **72**, 172501 (2005).
[15] E. Bauer, H. Kaldarar, R. Lackner, H. Michor, W. Steiner, E. W. Scheidt, A. Galatanu, F. Marabelli, T. Wazumi, K. Kumagai, and M. Feuerbacher, Phys. Rev. B **76**, 014528 (2007).

[16] E. Bauer, G. Rogl, X.-Q. Chen, R. T. Khan, H. Michor, G. Hilscher, E. Royanian, K. Kumagai, D. Z. Li, Y. Y. Li, R. Podloucky, and P. Rogl, Phys. Rev. B **82**, 064511 (2010).
[17] V. P. Mineev and Y. Yoshioka, Phys. Rev. B **81**, 094525 (2010).
[18] V. M. Edelstein, Phys. Rev. B **83**, 113109 (2011).
[19] D. Puggioni and J. M. Rondinelli, Nat. Commun. **5**, 3432 (2014).
[20] Z. Wang, Y. He, M. Gu, Y. Du, S. X. Mao, and C. Wang, ACS Appl. Mater. Interfaces **8**, 24567 (2016).
[21] R. E. Cohen, Nature **358**, 136 (1992).
[22] K. C. Pitike, W. D. Parker, L. Louis, and S. M. Nakhmanson, Phys. Rev. B **91**, 035112 (2015).
[23] X. He and K.-j. Jin, Phys. Rev. B **94**, 224107 (2016).
[24] C. Ma, X. He, and K.-j. Jin, Phys. Rev. B **96**, 035140 (2017).
[25] J.-x. Gu, K.-j. Jin, C. Ma, Q.-h. Zhang, L. Gu, C. Ge, J.-s. Wang, C. Wang, H.-z. Guo, and G.-z. Yang, Phys. Rev. B **96**, 165206 (2017).
[26] K. J. Choi, M. Biegalski, Y. L. Li, A. Sharan, J. Schubert, R. Uecker, P. Reiche, Y. B. Chen, X. Q. Pan, V. Gopalan, L.-Q. Chen, D. G. Schlom, and C. B. Eom, Science **306**, 1005 (2004).
[27] J. Wang, J. B. Neaton, H. Zheng, V. Nagarajan, S. B. Ogale, B. Liu, D. Viehland, V. Vaithyanathan, D. G. Schlom, U. V. Waghmare, N. A. Spaldin, K. M. Rabe, M. Wuttig, and R. Ramesh, Science **299**, 1719 (2003).
[28] L. Liu, H. Guo, H. Lü, S. Dai, B. Cheng, and Z. Chen, J. Appl. Phys. **97**, 054102 (2005).
[29] Y. Shao, R. A. Hughes, A. Dabkowski, G. Radtke, W. H. Gong, J. S. Preston, and G. A. Botton, Appl. Phys. Lett. **93**, 192114 (2008).
[30] Y. Iwazaki, T. Suzuki, Y. Mizuno, and S. Tsuneyuki, Phys. Rev. B **86**, 214103 (2012).
[31] Y. Wang, X. Liu, J. D. Burton, S. S. Jaswal, and E. Y. Tsymbal, Phys. Rev. Lett. **109**, 247601 (2012).
[32] K. Page, T. Kolodiazhnyi, T. Proffen, A. K. Cheetham, and R. Seshadri, Phys. Rev. Lett. **101**, 205502 (2008).
[33] T. Kolodiazhnyi, M. Tachibana, H. Kawaji, J. Hwang, and E. Takayama-Muromachi, Phys. Rev. Lett. **104**, 147602 (2010).
[34] S. Raghavan, J. Y. Zhang, O. F. Shoron, and S. Stemmer, Phys. Rev. Lett. **117**, 037602 (2016).
[35] K. S. Takahashi, Y. Matsubara, M. S. Bahramy, N. Ogawa, D. Hashizume, Y. Tokura, and M. Kawasaki, Sci. Rep. **7**, 4631 (2017).
[36] See Supplemental Material at http://link.aps.org/supplemental/10.1103/PhysRevB.97.115103 for details of the computational details for DFT, the DOS of the $BaTiO_3$ total unit cell, and Ti 3*d* orbitals with various doping densities without strain; also see Refs. [35,37–40].
[37] J. P. Perdew, A. Ruzsinszky, G. I. Csonka, O. A. Vydrov, G. E. Scuseria, L. A. Constantin, X. Zhou, and K. Burke, Phys. Rev. Lett. **100**, 136406 (2008).
[38] G. Kresse and J. Furthmüller, Phys. Rev. B **54**, 11169 (1996).
[39] G. Kresse and D. Joubert, Phys. Rev. B **59**, 1758 (1999).
[40] K. Momma and F. Izumi, J. Appl. Crystallogr. **41**, 653 (2008).
[41] N. A. Pertsev, A. G. Zembilgotov, and A. K. Tagantsev, Phys. Rev. Lett. **80**, 1988 (1998).
[42] O. Diéguez, S. Tinte, A. Antons, C. Bungaro, J. B. Neaton, K. M. Rabe, and D. Vanderbilt, Phys. Rev. B **69**, 212101 (2004).
[43] N. Marzari and D. Vanderbilt, in *First-Priniciples Calculations for Ferroelectrics—1998, Williamsburg, VA, Proceedings of the 5th Williamsburg Workshop on First-Principles Calculations for Ferroelectrics*, edited by R. E. Cohen, AIP Conf. Proc. No. 436 (AIP, Woodbury, NY, 1998), p. 146.
[44] V. Polinger, P. Garcia-Fernandez, and I. B. Bersuker, Phys. B (Amsterdam, Neth.) **457**, 296 (2015).